*J. Fluid Mech.* (1970), *vol.* 40, *part* 3, *pp.* 481–493
*Printed in Great Britain*



# Induction velometry in a shock wave

By G. KAMIMOTO AND M. NISHIDA
Department of Aeronautical Engineering, Kyoto University, Japan

(Received 25 April 1969 and in revised form 28 July 1969)

This paper describes theoretical and experimental studies for induction velometry in a shock wave. The induced potential gradient profiles across the shock is obtained with an assumption that the velocity of the charged particles is given by Mott-Smith's result. The calculated result of the induced potential gradient shows that it is not proportional to the velocity of the charged particles, since eddy currents are also induced by the existence of non-uniform velocity through the shock. The induced potential gradient is measured across the shock produced by a shock holder. This result is compared with the theoretical result. The experimental result shows that the charged particles follow the Rankine–Hugoniot relation in the velocity.

## 1. Introduction

Electrically conducting material moving in a magnetic field experiences an electromotive force acting in a direction perpendicular to both the motion and the magnetic field. In other words, the electric potential is induced in the direction of the electromotive force, and is a function of both the magnetic field strength and the velocity. If both the magnetic field and velocity are uniform, the induced potential gradient is proportional to the velocity, and therefore, if the magnetic flux density and the potential gradient are known, the velocity can be estimated. However, if the magnetic field or velocity is not uniform, induced eddy currents exist. The potential difference picked up by the probes is determined not only by the local velocity of the flow, but is also influenced by the eddy current at the point in question. Therefore, the induced potential gradient is not proportional to the velocity.

Thürlemann (1941) and Kolin & Reiche (1954) analyzed theoretically the pipe flow, which had a radial distribution of velocity and was transverse to the magnetic field. They obtained the radial distribution of the induced potential gradient. Kolin (1943) measured the potential gradient in the radial direction. Boucher & Ames (1961) found that induced eddy currents existed due to the edge effect of the magnetic field even if the flow velocity was uniform. Recently, induction velometry has been used in a plasma jet wind tunnel and a shock tube where the gas behind a shock was ionized. Clayden (1964) obtained the velocity of the free stream in a plasma jet using it; however, he neglected the effect of eddy currents. Croce (1965) used induction velometry to detect the shock followed by ionization in a shock tube, and obtained the particle velocity behind the shock.

In this paper, we apply induction velometry to the flow across the shock. Since the velocity of the charged particles changes sharply across the shock, there exist eddy currents, and therefore the induced potential gradient will not be proportional to the velocity. We can estimate velocity profile of the charged particles across the shock by comparing the measured potential gradient profile with the theoretical one.

## 2. Expression of induced potential for model 1

The fluid is assumed to obey Ohm's law. The conductivity is isotropic and unaffected by the magnetic field or the fluid motion. When the magnetic field is steady, the current flow in the fluid is taken to be governed by Ohm's law in the form,

$$\mathbf{j}/\sigma = -\operatorname{grad}\phi + \mathbf{v}\times\mathbf{B}, \tag{1}$$

where $\sigma$ is the electrical conductivity, $\mathbf{j}$ is the current density, $\mathbf{v}$ is the fluid velocity, $\mathbf{B}$ is the magnetic flux density, and $\phi$ is the electric potential. Consider the

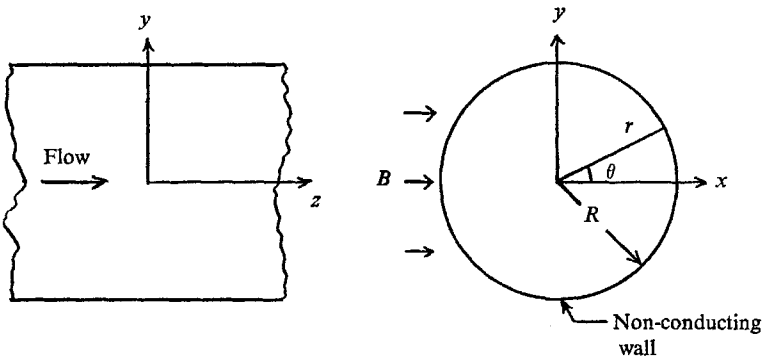


FIGURE 1. Partially ionized gas flow across a magnetic field.

case where there is a flow of the charged particles at velocity $v(z)$ in the $z$-direction in a pipe with non-conducting wall under a uniform field $B$ that is applied only in the $x$-direction as shown in figure 1. In our case,

$$v_r = v_\theta = 0, \quad v_z = v(z),$$

$$B_r = B\cos\theta, \quad B_\theta = -B\sin\theta, \quad B_z = 0.$$

In the above case, we can obtain the following component equations from (1) using cylindrical co-ordinates:

$$\frac{j_r}{\sigma} = -\frac{\partial\phi}{\partial r} - v_z B_\theta, \tag{2a}$$

$$\frac{j_\theta}{\sigma} = -\frac{1}{r}\frac{\partial\phi}{\partial\theta} + v_z B_r, \tag{2b}$$

$$\frac{j_z}{\sigma} = -\frac{\partial\phi}{\partial z}. \tag{2c}$$

Assuming that the electrical conductivity is uniform and substituting (2) into $\operatorname{div}\mathbf{j} = 0$ leads us to

$$\frac{1}{r}\frac{\partial}{\partial r}\left(r\frac{\partial\phi}{\partial r}\right)+\frac{1}{r^2}\frac{\partial^2\phi}{\partial\theta^2}+\frac{\partial^2\phi}{\partial z^2}=0. \tag{3}$$

We consider a model such as that shown in figure 2, where $v(z) = v$ for $z < z_0$ and $v(z) = 0$ for $z > z_0$. The boundary conditions for this model are

$$\frac{\partial\phi}{\partial z}=0, \quad \text{at} \quad \theta=0,\pi, \tag{4}$$

$$\frac{\partial\phi}{\partial z}=0, \quad \text{at} \quad z=\pm\infty, \tag{5}$$

$$\frac{\partial\phi}{\partial r}=0 \qquad \text{at} \qquad r=R \text{ in region 1}, \tag{6a}$$

$$\frac{\partial\phi}{\partial r}=Bv\sin\theta, \quad \text{at} \quad r=R \text{ in region 2}. \tag{6b}$$

Boundary condition (4) means that the $z$-component of eddy current does not exist at $\theta = 0, \pi$ due to the symmetry of the model with respect to the $x$–$z$ plane. Boundary condition (5) specifies no eddy currents in the $z$-direction at $z = \pm\infty$. Boundary conditions (6) are deduced from the condition that the normal component of eddy current does not exist at the wall.

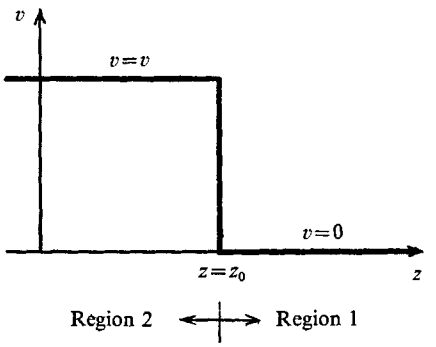


FIGURE 2. Model 1: $v(z) = v$ for $z < z_0$, $v(z) = 0$ for $z > z_0$.

Using the standard separation of variable technique, the following expression for $\phi$, which satisfies the boundary conditions and the condition that $\phi$ has a finite value at $r = 0$, are obtained:

$$\text{for } z > z_0, \qquad \phi_1 = A^{(1)}_{k,n}J_n(kr)\sin n\theta\exp(-kz), \tag{7}$$

$$\text{for } z < z_0, \qquad \phi_2 = A^{(2)}_{k,n}J_n(kr)\sin n\theta\exp(kz)+Bvr\sin\theta, \tag{8}$$

where $J_n(r)$ is a Bessel function, and $A^{(1)}_{k,n}$ and $A^{(2)}_{k,n}$ are arbitrary constants. And $k$ can be determined as follows: Boundary condition (6$a$) gives $J'_n(kR) = 0$. Putting $kR = \mu$, the solution for $J'_n(\mu) = 0$ are

$$\mu_{1,n}, \quad \mu_{2,n}, \quad \mu_{3,n}, \quad \ldots, \quad \mu_{m,n}, \quad \ldots \tag{9}$$

The values of the parameter $k$ corresponding to the values of $\mu$ are

$$k_{1,n}, \quad k_{2,n}, \quad k_{3,n}, \quad \ldots, \quad k_{m,n}, \quad \ldots. \tag{10}$$

Therefore, particular solutions are given by

$$\phi_1 = A^{(1)}_{m,n} J_n(k_{m,n} r) \sin n\theta \exp(-k_{m,n} z), \tag{11}$$

$$\phi_2 = A^{(2)}_{m,n} J_n(k_{m,n} r) \sin n\theta \exp(k_{m\ n} z) + Bvr \sin\theta. \tag{12}$$

General solutions are in the form,

$$\phi_1 = \sum_{m=1}^{\infty} \sum_{n=0}^{\infty} A^{(1)}_{m,n} J_n(k_{m,n} r) \sin n\theta \exp(-k_{m,n} z), \tag{13}$$

$$\phi_2 = \sum_{m=1}^{\infty} \sum_{n=0}^{\infty} A^{(2)}_{m,n} J_n(k_{m,n} r) \sin n\theta \exp(k_{m,n} z) + Bvr \sin\theta. \tag{14}$$

Now, $\phi$ is continuous across $z = z_0$ along with its first derivative, $\partial\phi/\partial z$; therefore

$$\sum_{m=1}^{\infty} \sum_{n=0}^{\infty} [A^{(1)}_{m,n} \exp(-k_{m,n} z_0) - A^{(2)}_{m,n} \exp(k_{m,n} z_0)] J_n(k_{m,n} r) \sin n\theta = Bvr \sin\theta, \tag{15}$$

$$A^{(1)}_{m,n} \exp(-k_{m,n} z_0) + A^{(2)}_{m,n} \exp(k_{m,n} z_0) = 0. \tag{16}$$

Since the left-hand side of (15) is a Fourier–Bessel series, the expansion coefficients are given by

$$A^{(1)}_{m,1} \exp(-k_{m,1} z_0) - A^{(2)}_{m,1} \exp(k_{m,1} z_0) = \frac{Bv \int_0^R J_1(k_{m,1} r)\, r^2\, dr}{\int_0^R [J_1(k_{m,1} r)]^2\, r\, dr}, \tag{17a}$$

$$A^{(1)}_{m,n} \exp(-k_{m,n} z_0) - A^{(2)}_{m,n} \exp(k_{m,n} z_0) = 0 \quad \text{for} \quad n \neq 1. \tag{17b}$$

From (16) and (17), we obtain the following expression:

$$A^{(1)}_{m,1} = \frac{Bv \exp(k_{m,1} z_0)}{2} \frac{\int_0^R J_1(k_{m,1} r)\, r^2\, dr}{\int_0^R [J_1(k_{m,1} r)]^2\, r\, dr}, \tag{18a}$$

$$A^{(2)}_{m,1} = -\frac{Bv \exp(-k_{m,1} z_0)}{2} \frac{\int_0^R J_1(k_{m,1} r)\, r^2\, dr}{\int_0^R [J_1(k_{m,1} r)]^2\, r\, dr}, \tag{18b}$$

$$A^{(1)}_{m,n} = A^{(2)}_{m,n} = 0 \quad \text{for} \quad n \neq 1. \tag{18c}$$

Using these coefficients in (13) and (14), we can obtain the following:

for $z > z_0$,

$$\phi_1(r, \theta, z) = \frac{Bv \sin\theta}{2} \sum_{m=1}^{\infty} \exp[-k_{m,1}(z - z_0)] J_1(k_{m,1} r) \frac{\int_0^R J_1(k_{m,1} r)\, r^2\, dr}{\int_0^R [J_1(k_{m,1} r)]^2\, r\, dr}, \tag{19}$$

for $z < z_0$,

$$\phi_2(r,\theta,z) = -\frac{Bv\sin\theta}{2}\sum_{m=1}^{\infty}\exp\left[k_{m,1}(z-z_0)\right]J_1(k_{m,1}r) \times \frac{\int_0^R J_1(k_{m,1}r)\,r^2\,dr}{\int_0^R [J_1(k_{m,1}r)]^2\,r\,dr} + Bvr\sin\theta. \tag{20}$$

## 3. Induced potential gradient for velocity profile across shock

We consider model 2 shown in figure 3. This problem can be solved by superposing induced potential due to elements of the velocity. The potential at $z = z_*$ induced by the first to the $p$th elements of the velocity can be obtained in the same manner as the induced potential in region 2 of figure 2. The potential at $z = z_*$ induced by the $(p+1)$th to the $r$th elements of the velocity can be obtained in

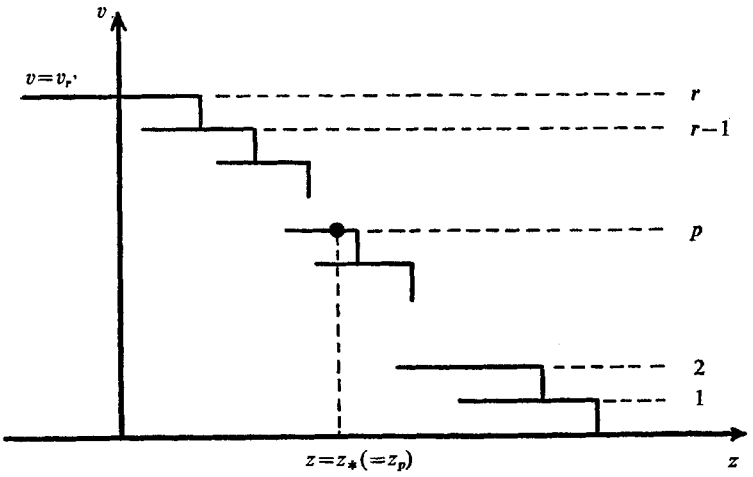


FIGURE 3. Model 2.

the same manner as the induced potential in region 1 of figure 2. Therefore, the potential at $z = z_*$ is given as follows:

$$\phi(r,\theta,z_*) = [\Delta\phi_2^{(1)} + \ldots + \Delta\phi_2^{(p)}] + [\Delta\phi_1^{(p+1)} + \ldots + \Delta\phi_1^{(r)}]. \tag{21}$$

$\Delta\phi_2$ and $\Delta\phi_1$ are obtained from (19) and (20) as follows:

$$\Delta\phi_2^{(f)} = \left[ -\frac{B\sin\theta}{2}\sum_{m=1}^{\infty}\exp\{k_{m,1}(z_f - z_*)\}J_1(k_{m,1}r) \times \frac{\int_0^R J_1(k_{m,1}r)\,r^2\,dr}{\int_0^R [J_1(k_{m,1}r)]^2\,r\,dr} + Br\sin\theta \right]\Delta v \quad (f = 1, 2, \ldots, p), \tag{22}$$

$$\Delta\phi_1^{(q)} = \left[ \frac{B\sin\theta}{2} \sum_{m=1}^{\infty} \exp\{-k_{m,1}(z_q - z_*)\} J_1(k_{m,1}r) \times \frac{\int_0^R J_1(k_{m,1}r)\, r^2\, dr}{\int_0^R [J_1(k_{m,1}r)]^2 r\, dr} \right] \Delta v \quad (q = p+1, p+2, \ldots, r), \tag{23}$$

where

$$\Delta v = \frac{v_r}{r}. \tag{24}$$

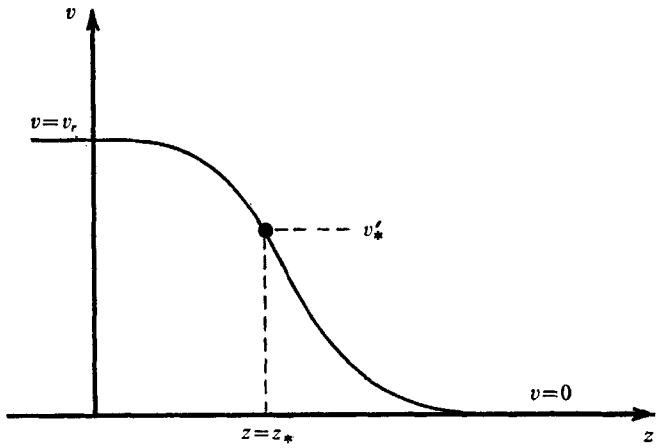


FIGURE 4. Model 3.

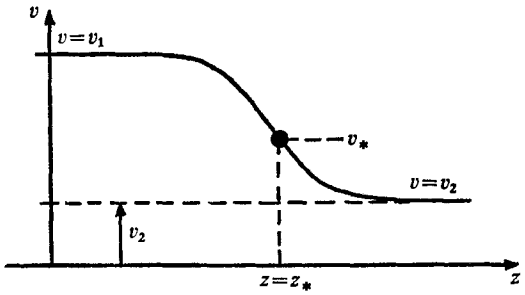


FIGURE 5. Model 4: velocity profile across a shock.

In the case of model 3, shown in figure 4, the potential at $z = z_*$ is given in integral form as follows:

$$\phi(r, \theta, z_*) = \int_0^{v_r - v'_*} d\phi_1 + \int_0^{v'_*} d\phi_2. \tag{25}$$

Finally, we consider such a model as shown in figure 5, which is similar to the velocity profile across the shock. Since the velocity profile in figure 5 is obtained by adding a uniform velocity $v_2$ to the velocity in model 3, the potential in model 4

can be obtained by superposing the potential $Bv_2 r\sin\theta$ induced by the velocity $v_2$ on (25). Therefore,

$$\phi(r,\theta,z_*) = \int_0^{v_1-v_*} d\phi_1 + \int_0^{v_*-v_2} d\phi_2 + Bv_2 r\sin\theta. \tag{26}$$

After using (19) and (20) in (26) and arranging, the following is obtained:

$$\begin{aligned}\phi(r,\theta,z_*) = Bv_* r\sin\theta + \frac{B\sin\theta}{2}\sum_{m=1}^{\infty} J_1(k_{m,1}r) \\ \times \frac{\int_0^R J_1(k_{m,1}r)\,r^2\,dr}{\int_0^R [J_1(k_{m,1}r)]^2\,r\,dr}\left[\int_0^{v_1-v_*}\exp\{-k_{m,1}(z_*-z)\}\,dv\right. \\ \left. -\int_0^{v_*-v_2}\exp\{k_{m,1}(z_*-z)\}\,dv\right],\end{aligned} \tag{27}$$

where $z$ is a function of $v$. Since we measure $\partial\phi/\partial y$ at $r=0$ across a shock, we must obtain the expression for $(\partial\phi/\partial r)_{\substack{r=0\\ \theta=\frac{1}{2}\pi}}$. The following non-dimensional quantities are introduced:

$$\left.\begin{aligned}\rho = r/R, \quad \xi = z/L, \quad \xi_* = z_*/L, \quad q = v/v_1, \\ q_* = v_*/v_1, \quad q_2 = v_2/v_1, \quad K = R/L,\end{aligned}\right\} \tag{28}$$

where $L$ is the maximum slope thickness of a shock, and $v_1$ and $v_2$ are the velocity upstream and downstream of the shock, respectively. Using these non-dimensional quantities and Bessel-function formulae, the non-dimensional potential gradient at $r=0$ is

$$\begin{aligned}\left[\frac{(\partial\phi/\partial r)_{\substack{r=0\\ \theta=\frac{1}{2}\pi}}}{Bv_1}\right]_{\xi=\xi_*} = q_* + \frac{1}{2}\sum_{m=1}^{\infty}\frac{\mu_{m,1}^2}{\mu_{m,1}^2-1}\frac{J_2(\mu_{m,1})}{[J_1(\mu_{m,1})]^2} \\ \times\left[\int_0^{1-q_*}\exp\left\{-\frac{\mu_{m,1}}{K}(\xi_*-\xi)\right\}dq - \int_0^{q_*-q_2}\exp\left\{\frac{\mu_{m,1}}{K}(\xi_*-\xi)\right\}dq\right].\end{aligned} \tag{29}$$

Clearly, the second term in the right-hand side of (29) expresses the effect of the eddy current.

## 4. Results of calculation

We assume that the velocity profile of the charged particles across the shock may be given by Mott-Smith's (1952) solution,

$$q = \frac{\exp(-4\xi)}{1+3\beta+\exp(-4\xi)}, \tag{30}$$

where

$$\beta = \frac{M^2-1}{M^2+3}, \tag{31}$$

in which $M$ is the Mach number upstream of the shock. Figure 6 shows the potential gradient profiles across the shock, which is obtained by using Mott-Smith's solution as the velocity profile. It is seen from this figure that the effect of the

eddy current is negligible when $K$ is small, which means that the maximum slope-thickness of a shock is sufficiently large in comparison with the diameter of the pipe.

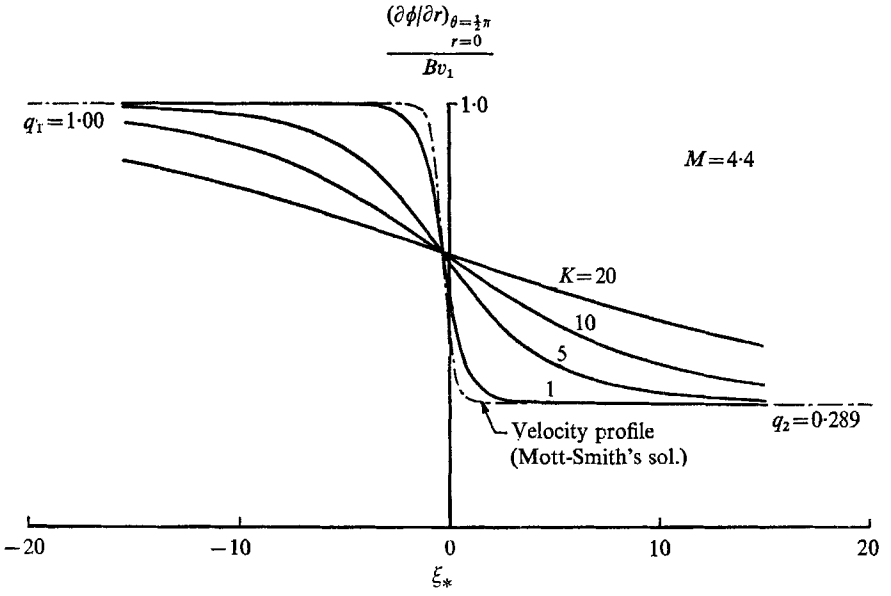


FIGURE 6. Effect of parameter $K$ upon potential gradient profile, $M = 4{\cdot}4$.

## 5. Experimental work and results

Experiments have been carried out in a test section of the Kyoto University Plasma Jet Wind Tunnel; they were reported by Kamimoto, Kimura & Teshima (1965), and Kamimoto & Nishida (1965). This wind tunnel is a continuous, open circuit tunnel, with an arc heater of 25 kW. It has a plenum chamber between the arc heater and the test section. Argon was used as a test gas. Typical conditions are shown below:

Mach number: 4·4;

electron number density: $4{\cdot}0 \times 10^{12}$ l/cm$^3$;

atom number density: $2{\cdot}0 \times 10^{15}$ l/cm$^3$;

electron temperature: 3400 °K.

The Mach number was obtained from the measurements of pitot pressure and stagnation pressure (plenum chamber pressure). Electron number density and electron temperature were measured by the Langmuir probe technique. Atom number density was calculated from stagnation temperature, stagnation pressure and Mach number. Stagnation temperature was obtained from the following relation (see appendix)

$$T_{0h} = \left(\frac{p_{0h}}{p_{0c}}\right)^2 T_{0c},$$

where $T_0$ and $p_0$ are stagnation temperature and stagnation pressure, respectively, and subscripts $h$ and $c$ represent the conditions when arc current is on (hot state) and off (cold state), respectively.

Since it is seen from the above-mentioned conditions that degree of ionization is of the order of $10^{-3}$, the present plasma is considered to be a partially ionized gas. Hence, the behaviour of the atoms is not influenced by that of the charged particles, and the charged particles follow the behaviour of the atoms. Therefore, it is expected that the charged particles have the same profile of the velocity across the shock as the atoms, and that they satisfy the Rankine–Hugoniot relation. So, measuring the potential gradient profile across the shock, we investigated whether the charged particles have the same velocity profile as the atoms and whether they satisfy the Rankine–Hugoniot relation.

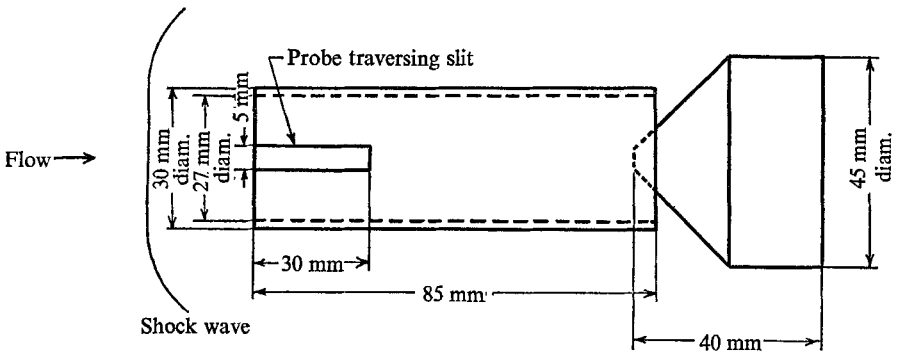


FIGURE 7. Shock holder made of pyrex glass.

The shock was produced by a shock holder, which is shown in figure 7. It was made of pyrex glass in order to insulate the shock holder electrically from the wind tunnel. A 30 mm-length slit was cut in the shock holder so that the probe measurement was possible behind the shock. Since the region where the potential gradient varies across the shock is very wide owing to the eddy currents resulted from the sharp variation of the velocity across the shock, the measurements have been made ranging from 50 mm upstream of the shock holder's entry plane to 50 mm downstream of it.

An electromagnet was used in order to produce a magnetic field. A current to the electromagnet was supplied by a battery and was changed with a variable resistance. A current of 1 amp gave the magnetic flux density of 15 Gauss.

The potential gradient was measured with probes which consisted of 0·5 mm diameter platinum wire. The voltage across the probes was recorded on an oscilloscope.

In order to measure the potential gradient locally, it is obviously desirable to have two probes as close as possible, but, since the probe consisted of wire of diameter $d$, an error of order $d/D$, where $D$ is the distance between the probe centres, could occur in the calculations for potential gradient. To eliminate this effect, an optimum distance $D$ between the probes was found. Figure 8 shows the voltage across the probes as a function of the distance between the probes. It is clear that the voltage across the probes for 25 mm distance is not linear. Since it

is desirable to have two probes as close as possible, $D$ was taken to be 10 mm. For $D = 10$ mm, $d/D$ is 5/100. An error of order 5/100 is allowable.

If a voltmeter with a resistance $\bar{R}$ is placed across the probes, then a current will flow, with the result that one probe will take on a voltage slightly higher than the floating potential and will collect an excess of electrons, whilst the other will be slightly lower than the floating potential and will collect an excess of ions, and

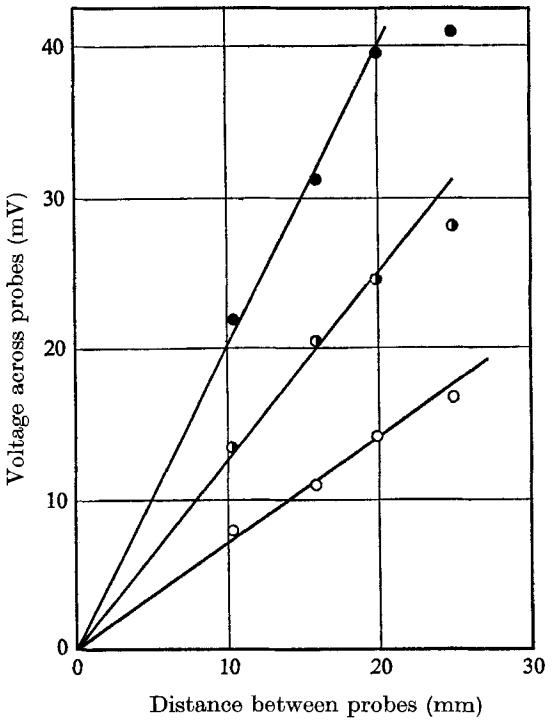


FIGURE 8. Voltage across probes as a function of distance between probes. ○, 10·2 Gauss; ◑, 15·3; ●, 22·9.

an error of voltage across the probes will occur. This error depends upon the resistance of the voltmeter. Clayden (1964) gave the following expression for the resistance:

$$\bar{R} \gg \frac{2kT_e}{eI_{i_{sat}}},$$

where $I_{i_{sat}}$ represents ion saturated current, $T_e$ electron temperature, $k$ Boltzmann constant and $e$ unit of electric charge. Since typically in the plasma jet, $T_e = 0{\cdot}3$ eV and $I_{i_{sat}} = 2$ mA,

$$\bar{R} \gg 300\,\Omega.$$

If a voltmeter with larger value of resistance than 300 Ω is used, the above-mentioned error can be eliminated. Since an oscilloscope with the resistance of 1 MΩ was used, the error due to the resistance was negligible.

Since the plasma jet has non-ionized surroundings, the boundary of the jet may be considered to be a non-conducting wall. Therefore, $R$, which represents

a diameter of a tube with a non-conducting wall, is taken to be a diameter of the plasma jet. In order to evaluate a parameter $K$, which is equal to $R/L$, the diameter of the plasma jet and the maximum slope thickness of the shock must be known. Muckenfuss (1960) obtained $l/L$, where $l$ is a mean free path for atom-atom collision ahead of the shock, as a function of Mach number. Using $l = 16\mu/5n_a(2\pi m_a kT_a)^{\frac{1}{2}}$, where $\mu$ is viscosity, $n_a$ the atom number density, $m_a$ the mass of the atom and $T_a$ the atom temperature, we can evaluate $L$ from Muckenfuss's result. $R$ was determined by measuring a radial distribution of ion-saturated current with a Langmuir probe. Thus, we can evaluate the parameter $K$.

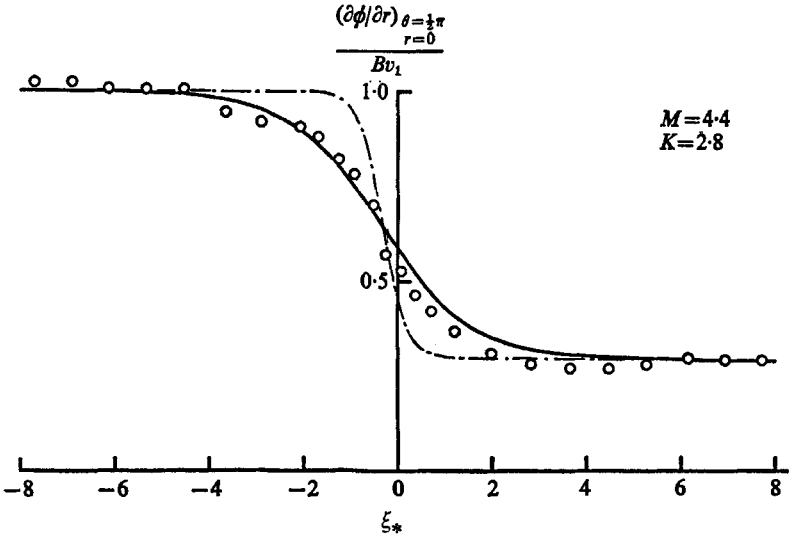


FIGURE 9. Comparison between theoretical and experimental results of induced potential gradient $M = 4{\cdot}4$, $n_a = 2{\cdot}0 \times 10^{15}$ 1/cm$^3$, $n_e = 4{\cdot}0 \times 10^{12}$ 1/cm$^3$, $T_e = 3400$ °K. ○, experiment; —, theory (equation (29)); —·—·—, velocity profile (Mott-Smith's solution).

The comparison between the experimental and theoretical results is shown in figure 9. On the assumption that the velocity of the charged particles is given by Mott-Smith's solution, the calculation for (29) was carried out by use of a digital computer HITAC 5020 (KDC-II). If the eddy current is neglected, the potential gradient will have the same profile as the velocity. However, the experimental result shows that the profile of the normalized potential gradient differs from that of the normalized velocity, in that, according to the present theory, the region where the potential gradient changes across the shock is wide compared with the region where the velocity changes. The experimental result agrees with the theoretical one, especially downstream of the shock. This agreement means that the charged particles are decelerated by the shock, and that, behind the shock, the velocity of them comes to the value given by the Rankine–Hugoniot relation. This behaviour across the shock is the same as the behaviour of the atoms. It also shows that uniform flow exists ahead of the shock.

## 6. Concluding remarks

In order to investigate whether the velocity of the charged particles should be given by Mott-Smith's solution or not, induction velometry was applied to the flow of the charged particles across the shock.

First, the theoretical investigation was carried out. The profiles of the potential gradient across the shock were calculated for several values of the parameter $K$. The results show that the effect of eddy currents on the profile of the potential gradient is negligible, if $K$ is small, which means that the maximum slope-thickness of the shock is sufficiently large compared with the diameter of the plasma jet. However, since the diameter of the plasma jet is generally larger than the maximum slope thickness of the shock, the profile of the potential gradient does not agree with that of the velocity. Hence, the measurement of the velocity by means of induction velometry seems impossible in a shock zone. However, if the calculated profile of the potential gradient is fitted to the measured profile, the velocity profile can be obtained.

In the second place, the potential gradient was measured across the shock, and the experimental result was compared with the theoretical. It is seen that behind the shock, the normalized value of the potential gradient approaches that of the downstream velocity given by the Rankine–Hugoniot relation. Hence, it is concluded that the charged particles are decelerated by the shock in the same way as the atoms, and that they satisfy the Rankine–Hugoniot relation. The experimental result shows that the measured profile of the potential gradient is similar to the theoretical one. We wish to propose that the velocity profile of the charged particles is close to that of the atoms only in a partially ionized gas.

## Appendix

Stagnation temperature can be estimated from the measurements of stagnation pressures as follows: Assuming that, for a given mass flow through a nozzle, the thickness of the boundary layer is independent of the temperature of the gas, we may write

$$\rho_h^* A^* a_h^* = \rho_c^* A^* a_c^*, \tag{A 1}$$

where $\rho^*$, $A^*$ and $a^*$ are density, cross-sectional area and sonic velocity at a nozzle throat, respectively, and the subscripts $h$ and $c$ show the conditions when the arc current is on (hot state) and off (cold state), respectively. Since

$$T_0 = \frac{\gamma+1}{2} T^*, \quad p_0 = \left(\frac{\gamma+1}{2}\right)^{\gamma/(\gamma-1)} p^*, \tag{A 2}$$

where $\gamma$ is a ratio of specific heat and the subscript 0 denotes stagnation condition, the following relation can be obtained:

$$\rho^* = \frac{p^*}{RT^*} = \frac{1}{R}\left(\frac{2}{\gamma+1}\right)^{\gamma/(\gamma-1)} \frac{p_0}{T_0}, \tag{A 3}$$

$$a^* = (\gamma R T^*)^{\frac{1}{2}} = \left(\frac{2\gamma}{\gamma+1} R T_0\right)^{\frac{1}{2}}. \tag{A 4}$$

Using (A 3) and (A 4) in (A 1),

$$T_{0h} = \left(\frac{p_{0h}}{p_{0c}}\right)^2 T_{0c}. \tag{A 5}$$

By measuring stagnation pressures for a given flow rate when the arc current is on and off, respectively, stagnation temperature for the hot state can be calculated from the above relationship, taking $T_{0c}$ as room temperature.

## REFERENCES


Boucher, A. R. & Ames, D. B. 1961 *J. Appl. Phys.* **32**, 755.

Clayden, W. A. 1964 *The High Temperature Aspects of Hypersonic Flow.* Oxford: Pergamon.

Croce, P. A. 1965 *Rev. Sci. Instrum.* **36**, 1561.

Kamimoto, G., Kimura, T. & Teshima, K. 1965 *Kyoto Univ. Aero. Eng. CP* no. 7.

Kamimoto, G. & Nishida, M. 1965 *Kyoto Univ. Aero. Eng. CP* no. 8.

Kolin, A. 1943 *J. Appl. Phys.* **15**, 150.

Kolin, A. & Reiche, F. 1954 *J. Appl. Phys.* **25**, 409.

Mott-Smith, H. M. 1952 *Phys. Rev.* **82**, 885.

Muckenfuss, C. 1960 *Phys. Fluids*, **3**, 320.

Thürlemann, B. 1941 *Helv. Phys. Acta*, **14**, 383.